DOI: 10.15849/IJASCA.231130.07

Int. J. Advance Soft Compu. Appl, Vol. 15, No. 3, November 2023
Print ISSN: 2710-1274, Online ISSN: 2074-8523

Design of Artificial Magnetic Conductor based Stepped V-shaped Printed multiband antenna for Wireless Applications

SatheeshKumar Palanisamy[1], Ghaida Muttashar Abdulsahib[2], Osamah Ibrahim Khalaf[3], Ajitha S S[4], Wing-Keung Wong[5], Shin-Hung Pan[6]

[1]Assistant Professor, Department of ECE, Coimbatore Institute of Technology, Coimbatore
e-mail: satheeshkumar.p@cit.edu.in
[2]Department of Computer Engineering,University of Technology, Baghdad, Iraq
e-mail: ghaida.m.abdulsaheb@uotechnology.edu.iq
[3]Department of Solar ,Al-Nahrain Research Center for Renewable Energy, Al-Nahrain University, Jadriya, Baghdad, Iraq
e-mail: usama81818@nahrainuniv.edu.iq
[4]TKM College of Engineering, Kollam, Kerala, India
ajithasubhadra@tkmce.ac.in
[5]Department of Finance, Fintech Center and Big Data Research Center
Asia University, Taiwan
e-mail: wong@asia.edu.tw
[6]Department of Information Management, Chaoyang University of Technology, Taiwan R.O.C
e-mail: vincentpan@cyut.edu.tw

Abstract

Antenna selection is a decision-making problem involving multiple factors, some of which may be at odds. This study aimed to develop a model for optimizing the design process for GSM mobile phone antennas. A 3.5GHz and 5.5GHz on-chip circularly polarized (C.P.) artificial magnetic conductor (AMC) based V-shaped stepped multiband 25x25mm^2 antenna has been designed and fabricated. The proposed antenna's profile height is much lower than antennas supported by traditional perfect electric conductor (PEC) ground planes due to careful tuning of the AMC reflector's reflection properties through optimization technique. According to simulated and observed data, the antenna presented in the proposal has the potential to achieve an impedance bandwidth of more than 45% (VSWR less than 1.8) while maintaining consistent radiation patterns across the frequency ranges 3.4 GHz to 5.86 GHz, 10.28 GHz to 11.86 GHz, and 13.69 GHz to 14.69 GHz. Measured analysis includes gain, radiation pattern, Axial Ratio, and return loss(S_{11}). The proposed antenna can be recommended for use in micro base station systems is suitable for this application because it possesses a low profile structure, an advantageously broad bandwidth, and the ease with which it can be manufactured.

Received 6 July 2023; Accepted 7 August 2023

Keywords: *Artificial Magnetic Conductor (AMC), defective ground structure, Genetic Algorithm, boresight, Coplanar waveguide, Quantitative Methods, Multiple Simultaneous Equation Models, Multiple Variable Model.*

1 Introduction

The swift evolution of integrated and versatile wireless communication systems has increased the need for multiband antennas, which can simultaneously cover multiple frequency bands. There is the possibility of using triple bands or dual bands [1], four sites [2], or penta bands [3-6]. In addition, methods that are plausible and suitable for the situation have been created. Techniques such as these slots [7], monopole arms [8], defective ground structure (DGS) [9, 10], engraved flaps [11], L-shaped slots [12], parasitic characteristics [13], and rectangular slots [14] are a few examples of the techniques that have been primarily identified in a study that has been published on this topic. Other examples include etching slits [11], rectangular slots [14], monopole arms [7], and slots [7, 8].

A frequency-based representation of anything and everything can be generated by applying many approaches, including complex permittivity and permeability. These qualities will determine how the material will behave when subjected to an electromagnetic environment. Left-handed or L.H. materials are a subtype of metamaterials characterized by negative permittivity and permeability. Left-handed materials are also generally referred to as L.H. materials. Occasionally, left-handed materials will be referred to as L.H. materials instead of left-handed ones. Some researchers working in the field of electromagnetics (E.M.) have modified the properties of lesser (L.H.) materials to acquire the suitable E.M. properties that are required for a variety of applications [15–16]. These metamaterials (MTM) have electromagnetic (E.M.) qualities that are unmatched by anything found in nature, and it is practically likely that nature will never produce them. Metamaterials[MTM] [17-24] offer increased versatility for constructing a wide variety of E.M. occurrences and direct the creation of structures composed of one or more unit cells. Providing a wide range of advantages is one way to accomplish this.

The antennas use one antenna or a considerable metallic ground, increasing their profile height—visible configuration. Low-profile antennas with good radiation performance have been designed using Artificial Magnetic Conductors (AMC) reflectors [17]. In [18], an antenna that is horizontally omnidirectional has a ground that is EBG and a profile height of 0.1 is described. Yet, the bandwidth is only 5.2% of the total. The research publication [19] describes a monopole antenna with an inkjet-printed AMC reflector. This antenna can attain a profile height of 0.0252.4 GHz throughout a 2.4–2.5 GHz frequency range.

This paper proposes an AMC-reflector-supported wideband, low-profile, dual-polarized, omnidirectional antenna. The antenna is described as having omni-directionality. An AMC reflector is included in the construction of the proposed antenna, in addition to a very high-performance monopole antenna and a high-performance loop antenna. The H.P. and V.P. omnidirectional antennas can be connected to generate a dual-polarized antenna if the AMC reflector's phase of reflection and other reflection properties

are precisely designed. This antenna is capable of simultaneously receiving signals coming from both directions.

2 Antenna Design

The design comprises two components: an antenna and an AMC. The design process is broken down into sections below, examining both parts of the whole. Copper is employed in this device for both the patch elements and the FR4, which requires the usage of a substrate.

2.1 AMC Design and Characterization

An AMC of periodic star unit cells that are eight by eight in size is utilized in this inquiry as a metallic reflector for rerouting radiations in the direction of a boresight for a monopole antenna. According to the design that has been proposed, there should be a grounded substrate that can hold a periodic lattice that has a periodicity of 10.8mm, as shown in Fig. 1c. This AMC does not contain any pins, eliminating the possibility of a short circuit between the ground plane and the patches. Low-cost FR-4 is utilized as the substrate, with a dielectric loss tangent ($\tan\delta$) of 0.025, permittivity(ε_r) of 4.3, and a thickness of 1.6 millimeters. An equivalent L.C. model, found in [11], is required to compute the unit cell proportions, as shown in Fig. 1

The floquet port excitation and unit cell boundary conditions were used to run the simulation. The AMC reflection phase diagram is depicted for your perusal in Figure 2, which may be found here. One of the many beneficial characteristics of this AMC is its capacity to provide zero reflection phase at a resonant frequency of 3.9 GHz. This AMC has a usable bandwidth that ranges between 2.1 and 4.8 GHz and is often contained within an area of 90 degrees on either side of the center frequency. AMC behaves like a perfect electric conductor (PEC) within the remaining frequency band. Consequently, the optimization strategies can be used to their full potential to acquire the desired operating band.

Ansys's built-in genetic Algorithm (G.A.) was utilized to fine-tune the unit cell's settings. Ansys employs in-built MATLAB control tools to determine the best possible unit cell dimensions. These GA-based optimizers are well-known for their sturdiness and their use of evolutionary principles [35]. Figure 3 is a flowchart taken from [36] that illustrates the steps taken by the suggested optimization technique. The AMC patch size (W_{amc}) and gap (g) have been defined as having ranges of 8 mm to 14 mm and 0.45 mm to 1.12 mm, respectively, as input variables.

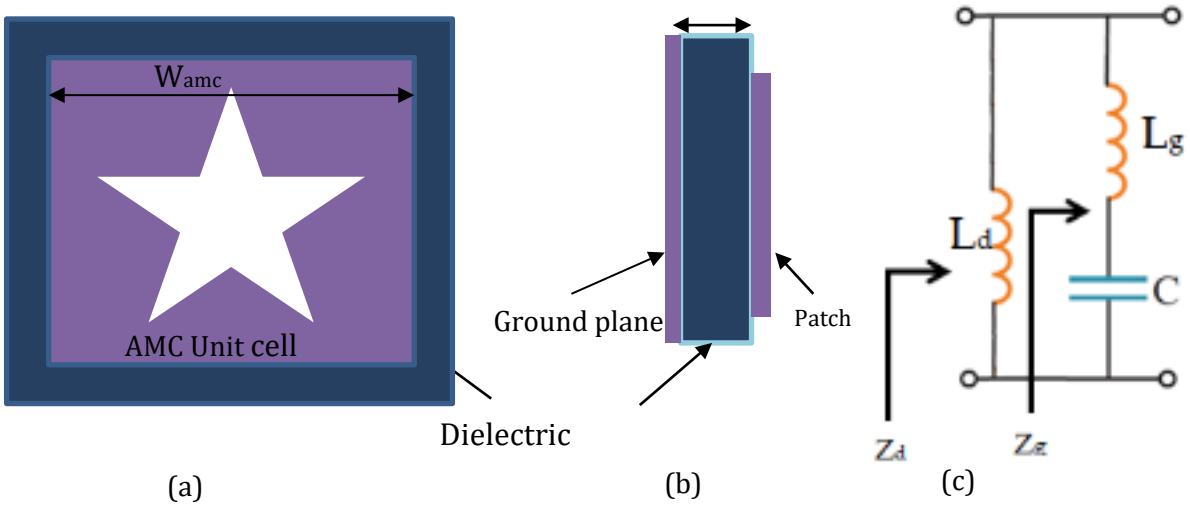

Figure 1 Analysis of AMC unit cell Characteristics (a) AMC unit cell; (b) side view of AMC unit cell; (c) Equivalent circuit of unit cell;

The AMC's relative permittivity and dimensions have been maintained at their original values. Eq. (1) [37] demonstrates how to define the fitness function for the target outcome. Fig. 1(c) shows the AMC's circuit model schematic. The formula for the overall surface impedance is calculated with respect to the equivalent circuit of unit cell in particular, shunt inductance connected directly across the terminals of the inductance and series capacitance as represented in equation (1):

$$Z_s(\omega) = Z_g \parallel Z_d = j\omega L_d \frac{1-\omega^2 L_g C_g}{1-\omega^2 (L_g + L_d) C_g} \quad . \qquad (1)$$

where, dielectric slab inductance (L_d), Grid inductance (L_g), and grid capacitance (C_g) are their corresponding electrical quantities. The grounded dielectric slab (Z_d) impedance is the inverse of the FSS grid impedance (Z_g). The formula makes it possible to calculate the resonance frequency of the structure. As the equivalent circuit parameters are calculated based on the desired frequency of resonance. The resonant frequency, circuit parameters are related using the expression (2). It is important to acknowledge that the validity of (1) and its related circuit model is contingent upon the isolation of from . In reference [7], it is demonstrated that the mushroom-like AMC [1] exhibits sufficient isolation when the cell size is not significantly larger than a general guideline.

$$f_r = \frac{1}{2\pi\sqrt{(L_g + L_d) C_g}} \quad . \qquad (2)$$

The model employed in this study is characterized by its simplicity, which unfortunately limits its ability to accurately forecast the impact of placing a PEC plane beneath the slab. Nevertheless, the advantage of the current model in comparison to its competitor's lies in its ability to incorporate the influence of the ground plane spacing on the variable d. In the subsequent section, we will elucidate the methodologies employed to get the AMC cell dimensions, specifically focusing on the dielectric slab inductance (Ld), grid inductance

(Lg), and grid capacitance (Cg). Two parallel patches placed on a dielectric slab of dielectric constant (ε_{eff}) and their grid capacitance, determined by

$$C_g = \frac{2W}{\pi} Cosh^{-1}(a/g)\varepsilon_0 \varepsilon_{reff}$$

$$\varepsilon_{reff} = \frac{\varepsilon_r + 1}{2} \quad . \qquad (3)$$

where W is the edge width, 'g' is the distance between two parallel structures, 'a' and 'g' represents broader dimensions of AMC, and gap 'g' between AMC elements.

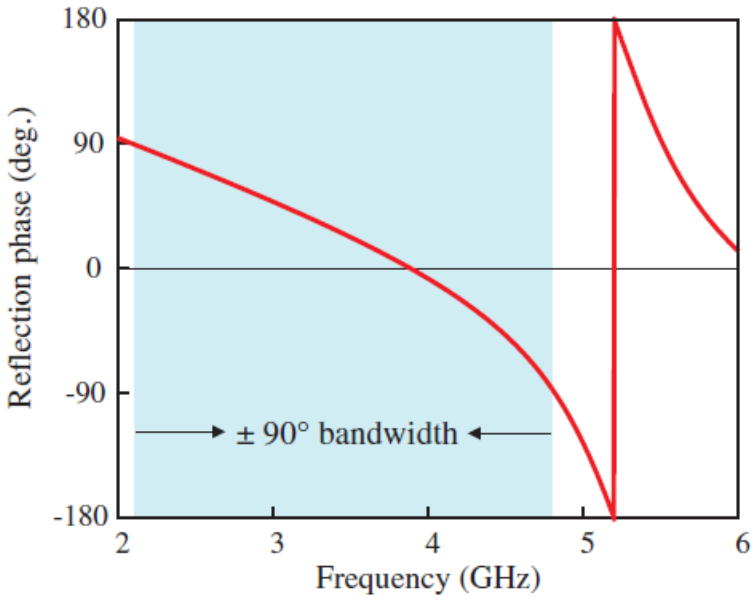

Figure 2: Representation of the Reflection phase for AMC unit cell

2.2 Implementation of AMC with Antenna Geometry and its parametrical study

The design model is depicted in Figure 4. The patch size, 19 mm by 9.5 mm, features a triangle carved into its center. It is fed via a coplanar waveguide and a microstrip line 8.8 millimeters in width and 3 millimeters in thickness. The dimensions of the object are 25 millimeters on each side. Creating the type requires utilizing an FR4 substrate with a value of 4.4. The thickness of the substrate is 1.6 millimeters, and its tan is 0.02. The ground must be close to the antenna's various components for a coplanar waveguide feed. The feed-to-ground spacing (often referred to as S_{fg}) is 0.4 millimeters. The geometrical dimensions of the proposed antenna are summarized in Table 1. Coplanar waveguide feed is used in the design process of antennas. The length and height of the wave port are taken into consideration while designing the port of wave on the antenna.

$$width = 2(2 * S_{fg} + W_f) . \quad (4)$$

where, W_f ground plane width, the objective is to cover a spectrum that may be used between 3 and 8.5 GHz and some area in the X-band. The proposed antenna frequency ranges from 3.4 GHz to 5.86 GHz, 10.28 GHz to 11.86 GHz, and 13.69 GHz to 14.28 GHz. Its resonance frequency is 4.6/11/13.9 GHz.

Since the only strict condition is the resonance frequency, the geometries naturally resemble the reference one and other well-known designs. The fitness function is straightforward here, with a single goal: to steer evolution toward a structure with the required resonant frequency. Finally, we might introduce an additional penalty coefficient to increase the bandwidth—an overlapping secondary objective. As predicted, smaller discretization step sizes increase the possibility that fitness generates local minima/maxima, which delays evolution.

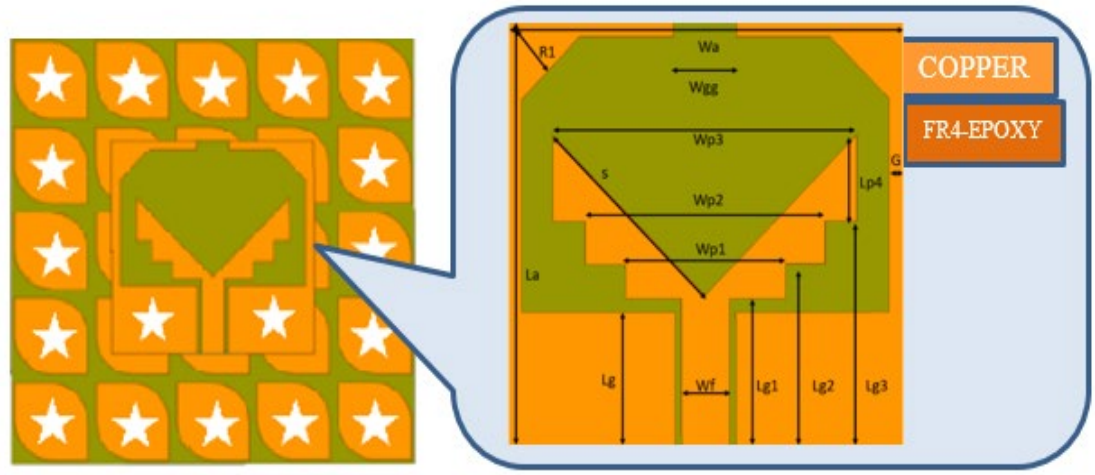

Figure 4 Geometry of the Proposed AMC Antenna

TABLE 1. Parametrical dimension of the proposed antenna (in mm)

Parameters	Dimension values	Parameters	Dimension values	Parameters	Dimension values	Parameters	Dimension values
R	4.5	W_c	10	W_f	3	S	13.3
R_1	4	W_{uc}	4.5	L_{g1}	8.8	L_s	50
L_c	10	W_{gg}	4	L_{g2}	10.8	W_s	50
L_g	8	W_{p1}	10	L_{g3}	13.3		
L_{uc}	4.5	W_{p2}	15	L_{p4}	5		
L_a	25	W_{p3}	19	G	1		

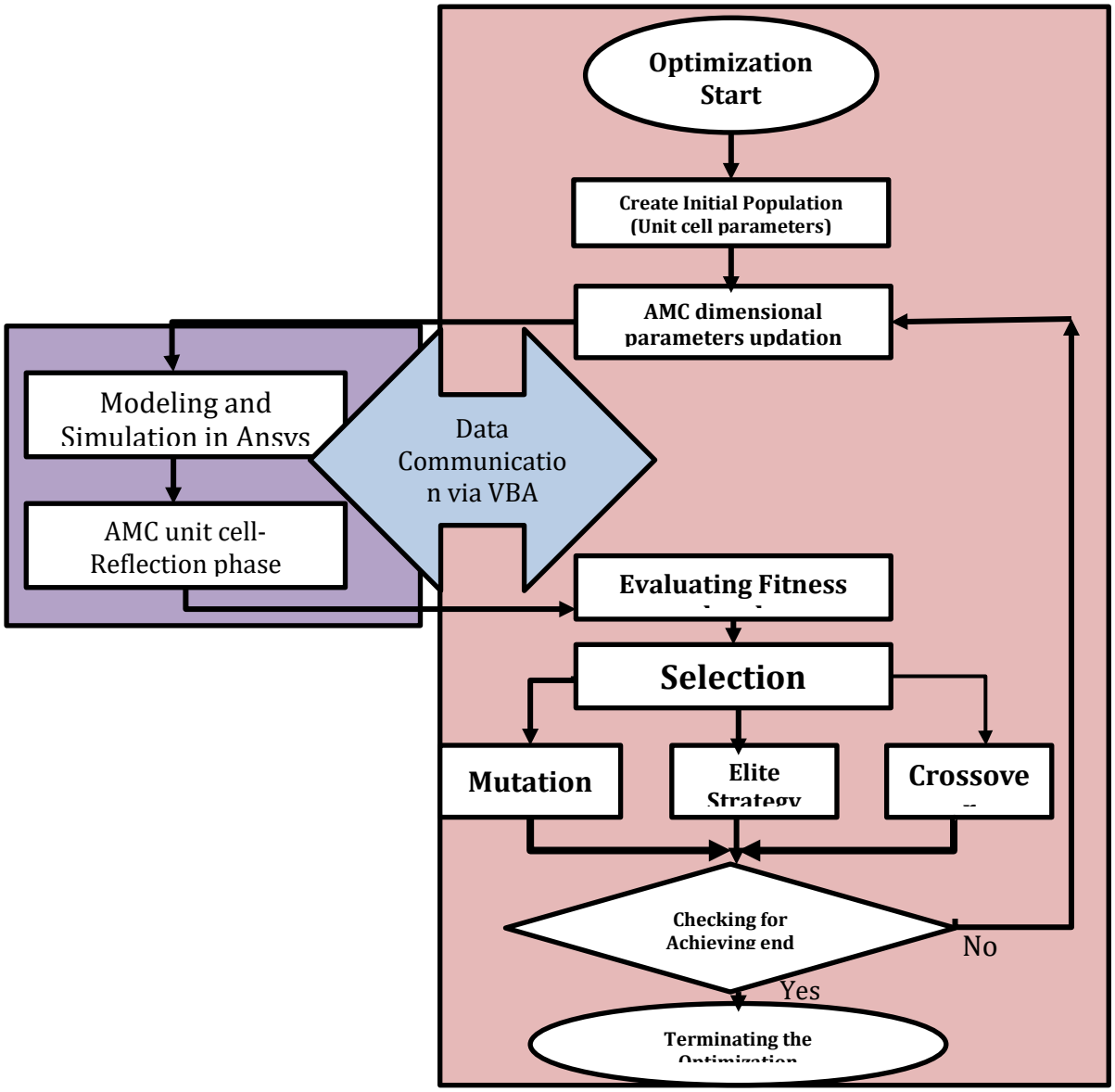

Fig. 3 Flowchart for the optimization of AMC unit cell through Genetic Algorithm

3 Results and Discussion

3.1 Circular Polarization

It is crucial first to describe the different ways that C.P. radiations can be formed before analyzing the C.P. process as it pertains to the current configuration of a monopole antenna. When it comes to C.P. radiation, a current distribution that results in the formation of a loop produces CP [33]. The CP mode is generated via a left-side coplanar ground plane that contains a quasi-loop formed by a rectangular etched slot. This plane also has a left-side coplanar ground plane. This channel makes it possible for the surface current to flow, and the direction of its arrows indicates that C.P. radiation is being produced. As a result,

it has right-hand circular polarization (RHCP) in the +z order, which is one of the senses associated with the C.P. modes.

3.2 Analysis of Parameters

In this part, we investigate how the performance of a monopole antenna varies depending on the length of the monopole (lm) and the coplanar gap (x). Monopole antennas' impedance matching and C.P. behavior are directly influenced by the optimal values chosen for their two most important parameters. While keeping all of the other parameters the same, the $|S_{11}|$ plots that correlate to the different changes in patch structure are displayed in Figure 5. Figure 5 shows that the $|S_{11}|$ is extremely sensitive to the shift in lm in the top band, but its sensitivity declines in the lower band. The higher band in the A.R. plot in Figure 6 significantly depends on l_m, whereas the lower band is only very slightly affected by it. In contrast, the lower band is highly dependent on the upper band.

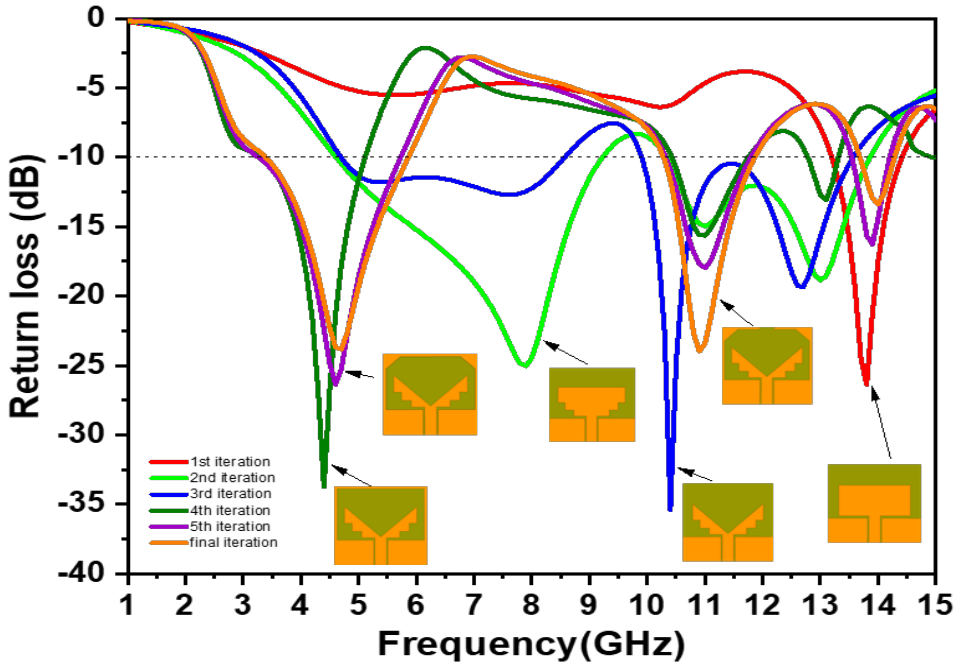

Figure 5 Comparative analysis of S_{11} of the antenna evolution

3.3 Return Loss

Using the HFSS tool Ansoft developed, the entire building was modeled and simulated. An Agilent E5071C network analyzer is utilized to measure the reflection coefficient. The findings from simulations have a high degree of concordance with the results from measurements. The impedance band measured at -10 dB extends from 2.1 to 2.87 Gigahertz (770 MHz) and 4.86 to 5.97 Gigahertz (1110 MHz) for the bottom and top bands. As a consequence of this, the antenna with an AMC structure that was recommended functions correctly across the entirety of the 2.4–2.5 GHz range.

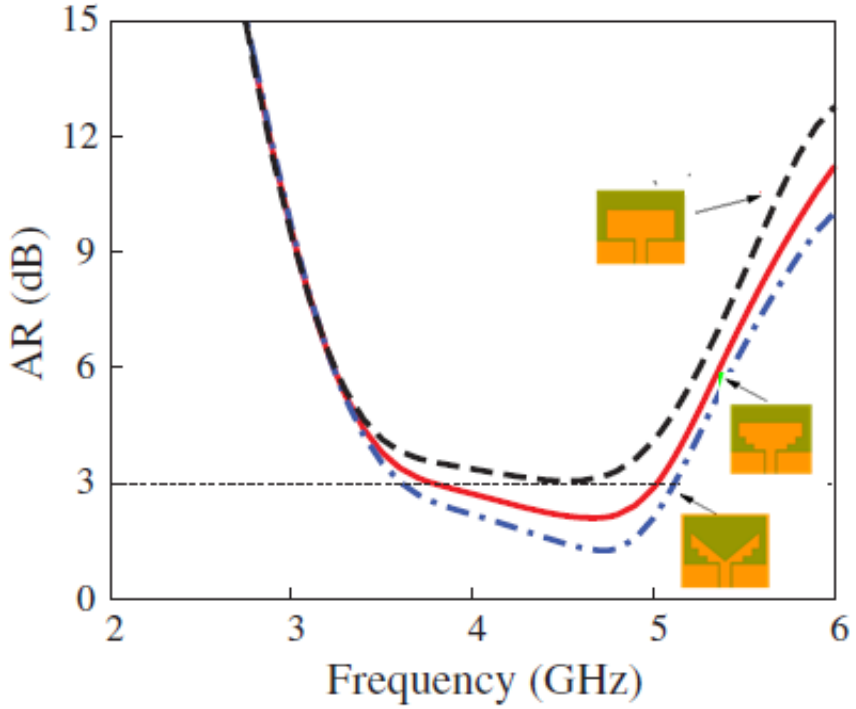

Fig.6 Comparative Analysis of Axial Ratio for proposed antenna structures

The completed model can operate in three distinct frequency bands, including the operating frequency that is being utilized at present. While the other two are cultivated as an outcome of ground connection and feeding.

3.4 Peak Gain

This antenna model can cover the frequency ranges of 3.4-5.86 GHz, 10.28-11.86 GHz, and 13.69 -14.28 GHz, thanks to its ability to operate simultaneously on three separate bands. Fig. 7 shows Gain variation without AMC. Between 2.8 GHz and 15 GHz, the antenna's gain is consistently positive over the whole frequency range.

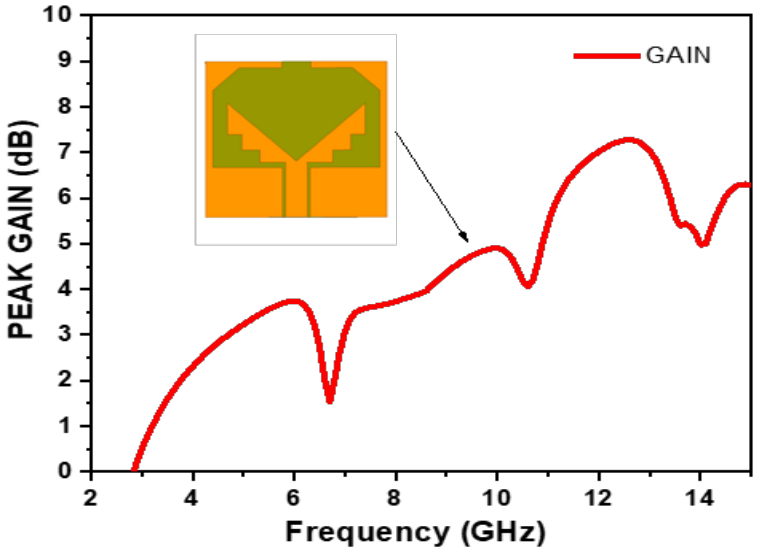

Figure 7 Gain plot Vs. Frequency (NO AMC)

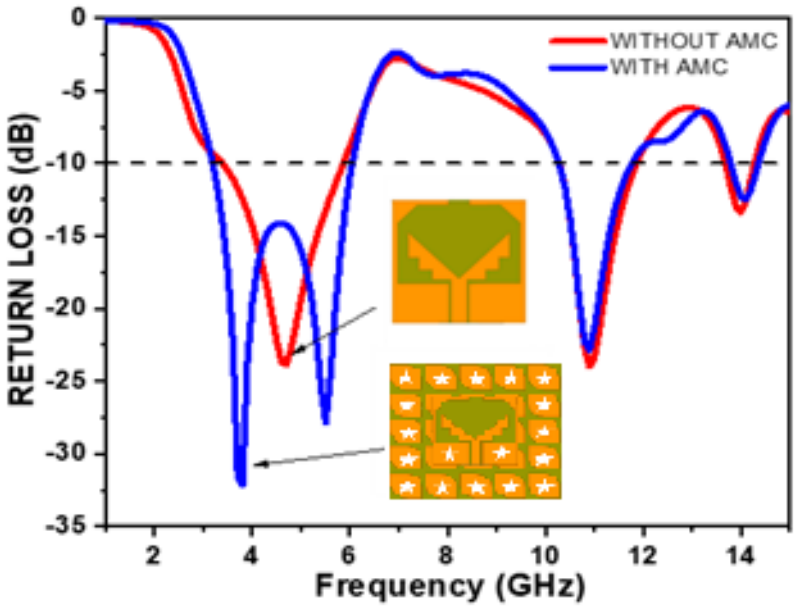

Figure 8 S_{11} plot AMC Vs. No AMC.

Figure 8 compares the Input reflection coefficient(S_{11}) for systems that do and do not use an artificial magnetic conductor (AMC). The red line represents systems lacking AMC, and the blue line represents systems with AMC. The ability to create an intense nulling level is a significant differentiator between this antenna and the ones discussed in [5-8, 10]. We switched the G.A. program's target value downward at regular intervals. Figure 9 depicts the actual nulling mode radiation patterns. To make things easier to see, we've transformed the -axis from 0 degrees to 360 degrees to 180 degrees and used Cartesian coordinates. The nulling levels are below 30 dBi at the ideal 0° and can rise as

high as 56.41 dBi at 2.7 GHz. These findings validate the proposed antenna's noise suppression and angular determination feasibility.

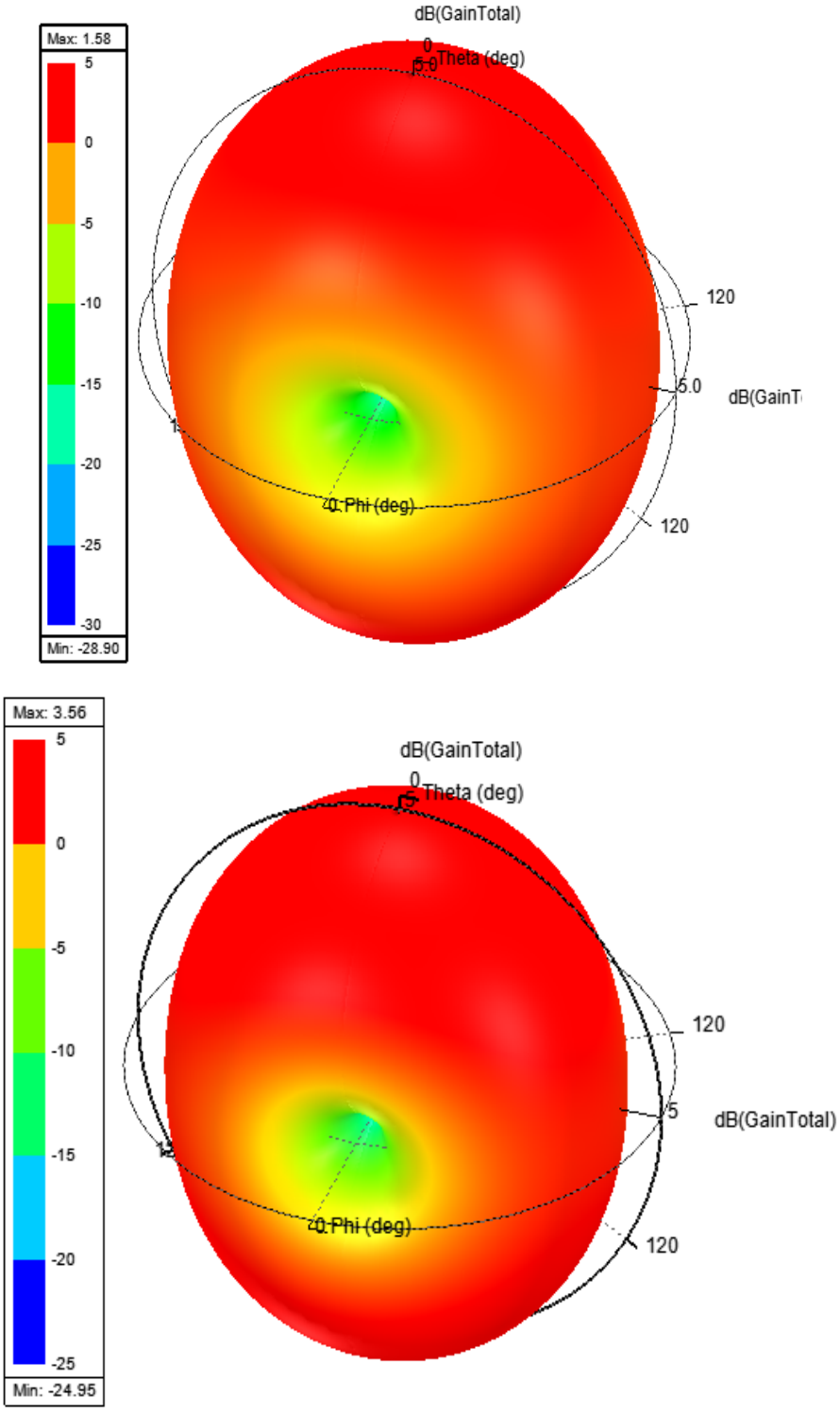

Figure 9. 4 Gain (NO AMC) @ 3.5 and 5.5 GHz

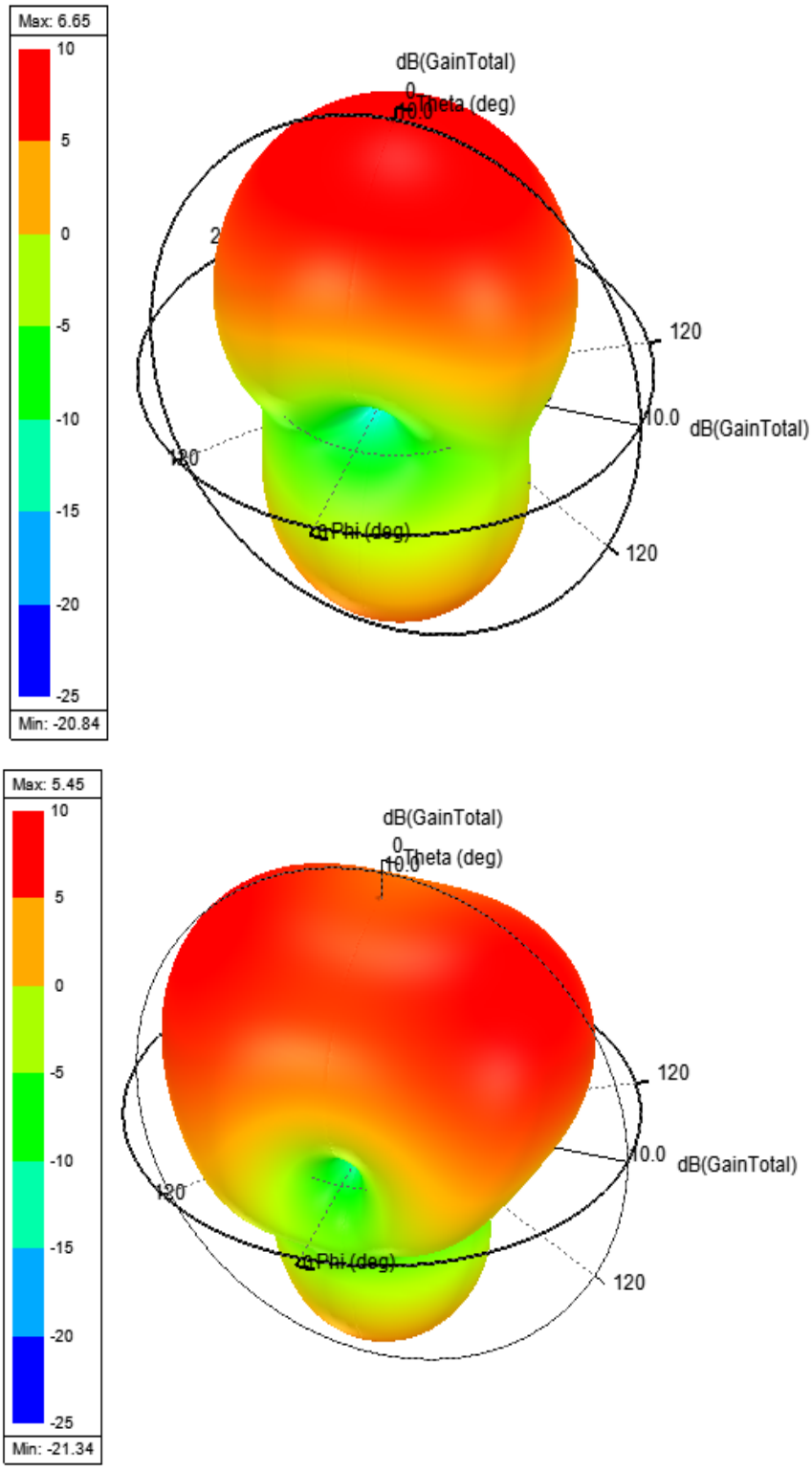

Figure 10 Gain (AMC) @ 3.5 and 5.5 GHz

Figures 9 and 10 show that the gain rises for both of the frequencies that were plotted and when one looks at the gain plot, one can see that the primary lobe is increasing while the lobe at the back is diminishing. As a result of the location of the AMC, the size of the back lobe has been minimized.

4 Conclusion

With the addition of CSRR and SRR structures, it is possible to set up a four-band arrangement that increases both gain and bandwidth, in addition to polarizing each of the four bands individually. The results of the measured tests and the simulated performance for the prototyped antenna agree reasonably well. PCS, GPS, DCS, Bluetooth/WLAN, UMTS, WiFi, and V2X are the four separate frequency bands an AMC-CPW multiband integrated antenna can service for usage with Bluetooth at 2.4 GHz, 5.8 GHz, and 3.35 GHz, WLAN and ISM compatibility with WiMAX, the application bands. WiMAX is one of the approved application bands. WiMAX also supports application bands located anywhere on the spectrum between 8 and 8.5 GHz. As the antenna, we utilized a wideband monopole configuration.

The AMC uses a star-shaped element, then topped by a wideband printed monopole spaced 3 millimeters above it. Altering the AMC's inner or outer square dimensions allows for independent tuning of the two AMC working frequency bands. The anechoic chamber radiation patterns resembled AMC antennas in the E and H planes. These patterns have higher forward gain and lower back radiation. Boresight gain rose to 1.1–7.9 dBi. A platform-tolerant multiband antenna system works well for vehicles, body-worn systems, and other applications. The extension of our paper could use advanced tools [20, 21, 22] to improve the work studied in the paper. Researchers could also apply this approach to investigate other areas, for example, economics and finance [23, 24, 25], decision sciences [26, 27, 28, 29], etc.

Acknowledgments:

The second author would like to thank Robert B. Miller and Howard E. Thompson for their continuous guidance and encouragement. This research has been supported by Asia University, China Medical University Hospital, The Hang Seng University of Hong Kong, the Research Grants Council (RGC) of Hong Kong (project numbers 12502814 and 12500915), and the Ministry of Science and Technology (MOST, Project Numbers 106-2410-H-468-002 and 107-2410-H-468-002-MY3), Taiwan.

Conflicts of Interest: The authors declare no conflict of interest.

REFERENCES

[1]. M. Zavvari, R. Ebadzadeh, and M. Mohammadifar, "Localized surface plasmons of a corrugated metal–insulator–metal ring resonator for enhanced multiband antenna," *Electron. Lett.,* vol. 54, no. 3, pp. 120– 122,Feb. 2018.

[2]. Xue, X.; Marappan, R.; Raju, S.K.; Raghavan, R.; Rajan, R.; Khalaf, O.I.; Abdulsahib, G.M. Modelling and Analysis of Hybrid Transformation for Lossless Big Medical Image Compression. *Bioengineering* 2023, 10,333. https://doi.org/10.3390/bioengineering10030333.

[3]. Y. F. Cao, S. W. Cheung, and T. I. Yuk, "A multiband slot antenna for GPS/WiMAX/WLAN systems," IEEE Trans. Antennas Propag., vol. 63,no. 3, pp. 952–958, Mar. 2015.

[4]. Xue, X.; Chinnaperumal, S.; Abdulsahib, G.M.; Manyam, R.R.; Marappan, R.; Raju, S.K.; Khalaf, O.I. Design and Analysis of a Deep Learning Ensemble Framework Model for the Detection of COVID-19 and Pneumonia Using Large-Scale CT Scan and X-ray Image Datasets. *Bioengineering* 2023, 10, 363. https://doi.org/10.3390/bioengineering10030363

[5]. AngurajKandasamy, SaravanakumarRengarasu, Praveen KittiBurri, SatheeshkumarPalanisamy, K. Kavin Kumar, Aruna Devi Baladhandapani, Samson AlemayehuMamo, "Defected Circular-Cross Stub Copper Metal Printed Pentaband Antenna", *Advances in Materials Science and Engineering,* vol. 2022, Article ID 6009092, 10 pages, 2022. https://doi.org/10.1155/2022/6009092

[6]. Iqbal M. Batiha, Suhaib A. Njadat, Radwan M. Batyha, Amjed Zraiqat, Amer Dababneh, Shaher Momani, Design fractional-order PID controllers for Single-Joint robot arm model, *International Journal of Advances in Soft Computing and its Application,* 14, 2(2022), 96-114.

[7]. Y. Gong, S. Yang, B. Li, Y. Chen, F. Tong and C. Yu, "Multiband and High Gain Antenna Using AMC Ground Characterized With Four Zero-Phases of Reflection Coefficient," in *IEEE Access*, vol. 8, pp. 171457-171468, 2020.doi: 10.1109/ACCESS.2020.3024982

[8]. H. Liu, J. Wang and X. Luo, "Flexible and compact AMC based antenna for WBAN applications," 2017 *IEEE International Symposium on Antennas and Propagation & USNC/URSI National Radio Science Meeting*, San Diego, CA, 2017, pp. 587-588, doi: 10.1109/APUSNCURSINRSM.2017.8072336.

[9]. Dash, Sonali, et al. "Artificial Intelligence Models for Blockchain-Based Intelligent Networks Systems: Concepts, Methodologies, Tools, and Applications." In *Handbook of Research on Quantum Computing for Smart Environments,* edited by Amit Kumar Tyagi, 343-363. Hershey, PA: IGI Global, 2023. https://doi.org/10.4018/978-1-6684-6697-1.ch019 .

[10]. Palanisamy, S, Thangaraju, B. Design and analysis of clover leaf-shaped fractal antenna integrated with stepped impedance resonator for wireless applications. *Int J Commun Syst.* 2022; 35(11):e5184. doi:10.1002/dac.5184

[11]. S. Shi, P. Yang, L. Zhou, and W. Chen, "Wideband planar dipole based on dual-layer artificial magnetic conductor," J. Eng., vol. 2019, no. 19,pp. 6180–6183, Oct. 2019.

[12]. Palanisamy S, Thangaraju B, Khalaf OI, Alotaibi Y, Alghamdi S. Design and Synthesis of Multi-Mode Bandpass Filter for Wireless Applications. Electronics. 2021; 10(22):2853. https://doi.org/10.3390/electronics10222853

[13]. V. K. Pandit and A. R. Harish, "Dual-band monopole antenna loaded with dual-band AMC for WLAN/WiMAX applications," 2016 International Conference on Emerging Trends in Communication Technologies (ETCT), Dehradun, 2016, pp. 1-3, doi: 10.1109/ETCT.2016.7882966.

[14]. Xue, X.; Shanmugam, R.; Palanisamy, S.; Khalaf, O.I.; Selvaraj, D.; Abdulsahib, G.M. A Hybrid Cross Layer with Harris-Hawk-Optimization-Based Efficient Routing for

Wireless Sensor Networks. *Symmetry* 2023, *15*, 438. https://doi.org/10.3390/sym15020438.

[15]. Palanisamy, Satheeshkumar, BalakumaranThangaraju, Osamah Ibrahim Khalaf, YouseefAlotaibi, SalehAlghamdi, and FawazAlassery. 2021. "A Novel Approach of Design and Analysis of a Hexagonal Fractal Antenna Array (HFAA) for Next-Generation Wireless Communication" Energies 14, no. 19: 6204. https://doi.org/10.3390/en14196204

[16]. Tiku, Moti L., Wing-Keung Wong, David C. Vaughan, Guorui Bian (2000). Time Series Models in Non-Normal Situations: Symmetric Innovations. *Journal of Time Series Analysis*, *21*(5), 571-596.

[17]. Bai, Zhidong, Huixia Liu, and Wing-Keung Wong. "Enhancement of the applicability of Markowitz's portfolio optimization by utilizing random matrix theory." *Mathematical Finance: An International Journal of Mathematics, Statistics and Financial Economics* 19.4 (2009): 639-667.

[18]. Bai, Zhidong, Hua Li, Huixia Liu and Wing-Keung Wong, 2011, Test Statistics for Prospect and Markowitz Stochastic Dominances with Applications, Econometrics Journal 14(2), 278-303.

[19]. Maydybura, Alina, Raheel Gohar, Asma Salman, Wing-Keung Wong, Bisharat Hussain Chang, 2022. The Asymmetric Effect of the Extreme Changes in the Economic Policy Uncertainty on the Exchange Rates: Evidence from Emerging Seven Countries, Annals of Financial Economics, 2250031.

[20]. Wong, Wing-Keung, David Yeung, and Richard Lu. "The mean-variance rule for investors with reverse S-shaped utility." *Annals of Financial Economics* (2022): 2250030.

[21]. Obrimah, Oghenovo A., and Wing-Keung Wong. "Modeling of stock returns in continuous vis-á-vis discrete time is equivalent, respectively, to the conditioning of stock returns on a random walk process for trade imbalances vis-á-vis a random walk process for evolution of information." *Annals of Financial Economics* 17.02 (2022): 2250010.

[22]. Alghalith, Moawia, and Wing-Keung Wong. "Option Pricing Under an Abnormal Economy: using the Square Root of the Brownian Motion." *Advances in Decision Sciences* 26 (2022): 1-14.

[23]. Noman, Muhammad, Nguyen Duy Suu, Ho Thuy Tien, Do Thi Thanh Nhan, Shin-Hung Pan, Wing-Keung Wong. (2023). Impact of foreign ownership and foreign bank presence on liquidity risk: Evidence from Viet Nam. *Advances in Decision Sciences*, *27*(1), 23-44.

[24]. P. Satheesh Kumar and S. Valarmathy, "Development of a novel algorithm for SVMBDT fingerprint classifier based on clustering approach," *IEEE-International Conference On Advances In Engineering, Science And Management (ICAESM -2012)*, 2012, pp. 256-261.

[25]. K. Suganyadevi, V. Nandhalal, S. Palanisamy and S. Dhanasekaran, "Data Security and Safety Services using Modified Timed Efficient Stream Loss-Tolerant Authentication in Diverse

Models of VANET," *2022 International Conference on Edge Computing and Applications (ICECAA)*, 2022, pp. 417-422, doi: 10.1109/ICECAA55415.2022.9936128.

[26]. P. S. Kumar, S. Boopathy, S. Dhanasekaran and K. R. G. Anand, "Optimization of Multiband Antenna for Wireless Communication Systems using Genetic Algorithm," *2021 International Conference on Advancements in Electrical, Electronics, Communication, Computing and Automation (ICAECA)*, 2021, pp. 1-6, doi: 10.1109/ICAECA52838.2021.9675686.

[27]. Pham, Quoc Hai, Diep Ho, Sarod Khandaker, Anh Tung Tran (2022). Investigating the effects of Accounting Law on the Credit Rating Models using Artificial Neural Networks: a study in Vietnam. *Advances in Decision Sciences*, *26*(4), 1-32.

[28]. E. Suganya, T. Prabhu, Satheeshkumar Palanisamy, Praveen Kumar Malik, Naveen Bilandi, Anita Gehlot, "An Isolation Improvement for Closely Spaced MIMO Antenna Using λ/4 Distance for WLAN Applications", *International Journal of Antennas and Propagation*, vol. 2023, Article ID 4839134, 13 pages, 2023. https://doi.org/10.1155/2023/4839134.

[29]. A. P. Mukti, L. Lusiana, D. Titisari, and S. Palanisamy, "Performance Analysis of Twelve Lead ECG Based on Delivery Distance Using Bluetooth Communication", j.electron.electromedical.eng.med.inform, vol. 5, no. 1, pp. 46-52, Jan. 2023.

[30]. Sam P.J.C., Surendar U., Ekpe U.M., Saravanan M., Satheesh Kumar P. (2022) A Low-Profile Compact EBG Integrated Circular Monopole Antenna for Wearable Medical Application. In: Malik P.K., Lu J., Madhav B.T.P., Kalkhambkar G., Amit S. (eds) *Smart Antennas. EAI/Springer Innovations in Communication and Computing.* Springer, Cham.https://doi.org/10.1007/978-3-030-76636-8_23.

[31]. Satheesh Kumar, P., Jeevitha, Manikandan (2021). Diagnosing COVID-19 Virus in the Cardiovascular System Using ANN. In: Oliva, D., Hassan, S.A., Mohamed, A. (eds) *Artificial Intelligence for COVID-19. Studies in Systems, Decision and Control*, vol 358.Springer, Cham.https://doi.org/10.1007/978-3-030-69744-0_5.

[32]. S, D.; Palanisamy, S.; Hajjej, F.; Khalaf, O.I.; Abdulsahib, G.M.; S, R. Discrete Fourier Transform with Denoise Model Based Least Square Wiener Channel Estimator for Channel Estimation in MIMO-OFDM. *Entropy* 2022, 24, 1601. https:// doi.org/10.3390/e24111601.

[33]. Ravinagarajan, Janani, and Sharon Sophia. "Empirical Significance of Movements in Stock Trading Platforms in NSE Market Structure." *Advances in Decision Sciences* 26.3 (2022): 1-25.

[34]. Nivethitha, T., Palanisamy, S. K., MohanaPrakash, K., &Jeevitha, K. (2021).Comparative study of ANN and fuzzy classifier for forecasting electrical activity of heart to diagnose Covid-19. Materials today. Proceedings, 45, 2293–2305. https://doi.org/10.1016/j.matpr.2020.10.400.

[35]. SatheeshKumar & Balakumaran T. (2021). Modeling and simulation of dual layered U-slot multiband microstrip patch antenna for wireless applications. Nanoscale Reports, 4(1), 15 – 18. https://doi.org/10.26524/nr.4.3.

[36]. Palanisamy, S. (2022).Predictive Analytics with Data Visualization. Journal of Ubiquitous Computing and Communication Technologies, 4(2), 75-96. doi:10.36548/jucct.2022.2.003.

[37]. Raad Z. Homod et al., "Deep clustering of Lagrangian trajectory for multi-task learning to energy saving in intelligent buildings using cooperative multi-agent," in Applied Energy , Volume 351, 1 December 2023, 121843, doi.org/10.1016/j.apenergy.2023.121843.

[38]. Xingsi Xue et al., "A Novel partial sequence technique based Chaotic biogeography optimization for PAPR reduction in eneralized frequency division multiplexing waveform," in Heliyon, vol. 9, 2023, doi.org/10.1016/j.heliyon.2023.e19451.

[39]. S. K. Rana et al., "Decentralized Model to Protect Digital Evidence via Smart Contracts Using Layer 2 Polygon Blockchain," in IEEE Access, vol. 11, pp. 83289-83300, 2023, doi: 10.1109/ACCESS.2023.3302771.

[40]. Oshamah Ibrahim Khalaf,Ashokkumar. S.R,S.Dhanasekaran,Ghaida Muttashar Abdulsahib and Premkumar. A DECISION SCIENCE APPROACH USING HYBRID EEG FEATURE EXTRACTION AND GAN-BASED EMOTION CLASSIFICATION. Advances in Decision Sciences, 2023,Vol 27.https://doi.org/10.47654/v27y2023i1p172-191.Pages 172-191 .

[41]. Bisharat Hussain Chang,Khalil Ahmed Channa,Emmanuel Ucheand Osamah Ibrahim Khalaf. Analyzing The Impacts of Terrorism on Innovation Activity:A Cross-Country Empirical Study. Advances in Decision Sciences, 2023,Vol 26 .https://doi.org/10.47654/v26y2022i5p124-161.Pages 124-161 .

[42]. Ziqiang Tang et al. Machine Learning Assisted Energy Optimization in Smart Grid for Smart City Applications.Journal of Interconnection Networks, VOL. 22, NO. Supp03. https://doi.org/10.1142/S0219265921440060

[43]. S. Goswami, A. K. Sagar, P. Nand and O. I. Khalaf, "Time Series Analysis Using Stacked LSTM Model for Indian Stock Market," 2022 IEEE IAS Global Conference on Emerging Technologies (GlobConET), Arad, Romania, 2022, pp. 399-405, doi: 10.1109/GlobConET53749.2022.9872386.